ACS APPLIED MATERIALS & INTERFACES

Research Article

www.acsami.org

Flexibility and Color Monitoring of Cellulose Nanocrystal Iridescent Solid Films Using Anionic or Neutral Polymers

Raphael Bardet, Naceur Belgacem, and Julien Bras*

Univ. Grenoble Alpes, LGP2, F-38000 Grenoble, France

CNRS, LGP2, F-38000 Grenoble, France

LGP2/Grenoble INP-Pagora/CNRS - 461 rue de la papeterie, Domaine Universitaire, BP 65, 38402 Saint Martin d'Hères cedex, France

Supporting Information

ABSTRACT: One property of sulfated cellulose nanocrystals (CNCs) is their ability to self-assemble from a concentrated suspension under specific drying conditions into an iridescent film. Such colored films are very brittle, which makes them difficult to handle or integrate within an industrial process. The goal of this study is (i) to produce flexible films using neutral poly(ethylene glycol) (PEG) and (ii) to modulate their coloration using an anionic polyacrylate (PAAS). The first part is dedicated to studying the physicochemical interactions of the two polymers with CNCs using techniques such as zeta potential measurements, dynamic light scattering (DLS), quartz crystal microbalance (QCM), and atomic force microscopy (AFM). Iridescent solid films were then produced and characterized using scanning electron microscopy (SEM) and UV−visible spectroscopy. The mechanical and thermal properties of films incorporating CNC were measured to evaluate improvements in flexibility. The addition of 10 wt % of PEG makes these films much more flexible (with a doubling of the elongation), with the coloration being preserved and the temperature of degradation increasing by almost 35 °C. Up to 160 μmol/g_{CNC} PAAS can be added to tune the coloration of the CNC films by producing a more narrow, stronger coloration in the visible spectrum (higher absorption) with a well-pronounced fingerprint texture.

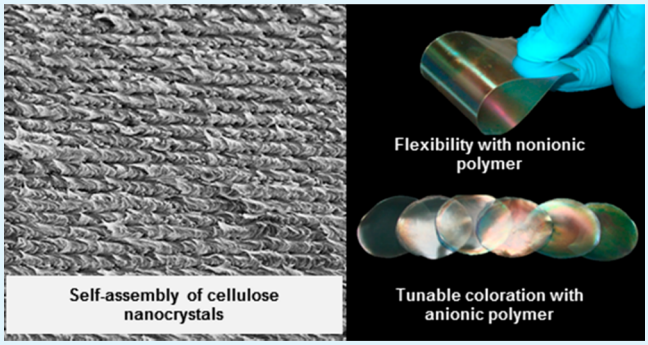

KEYWORDS: *cellulose nanocrystal, self-assembly, structural color, flexible iridescent films, polymer additives*

INTRODUCTION

In contrast to common pigment coloration, some surfaces appear colored only because of the interaction between light and their microstructure. This is known as structural coloration, and iridescence associated with this phenomenon is a major field of investigation.[1] Iridescence is an optical phenomenon that has fascinated artists, inventors, and scientists including Aristotle, Newton, and Darwin, for millennia and through the current day.[2] This amazing property of surfaces that change color with illumination or observation angle is found in nature. It can be observed in some animals,[3,4] such as the figeater beetle, turquoise emperor butterfly, and satin bowerbird, as well as some plants,[5−7] such as hibiscus trionum flowers, the tulipa species, and pollia condensata. Progress in engineering nanostructures has enabled the mimicry of nature for applications within many fields, such as display technologies, painting, printing, textiles, and cosmetics.[8,9]

Since 2010, the use of biobased nanomaterials for the design of photonic nanostructures has become a promising prospect in the field of optical encryption technology.[10,11] Cellulose nanocrystals (CNCs) are one of the most promising biobased nanomaterials, as exhibited by growing interest at the industrial scale following the recent construction of the first CNC processing plants in 2011 and the growth of the patent portfolio since 2008.[12]

These rod-like nanoparticles (approximately 5 nm wide and 250 nm in length) extracted from vegetal biomass (e.g., wood pulp) feature an attractive combination of properties including being biobased, biodegradable, and biocompatible. They also have a low density (∼1.6), high stiffness (∼150 GPa), high thermal stability (∼300 °C), and high density of hydroxyl groups that enables chemical modification and self-organization.[13] This study will focus only on the self-organization properties of CNC; more detailed information on the production, characterization, and utilization of CNC can be found in recent books[14] and reviews.[15−17] Recent works not only describe the characterization and production of CNC but also address its end use in smart applications, including

Received: October 13, 2014
Accepted: December 31, 2014
Published: December 31, 2014

DOI: 10.1021/am506786t
ACS Appl. Mater. Interfaces 2015, 7, 4010−4018

controlled drug release, as aerogels for insulation, as stimuli-responsive materials, and as photonic films.[18]

Due to the well-known property of CNCs to display liquid-crystalline behavior in water,[19] one outstanding application is the manufacturing of iridescent materials, as patented in 1995 by Revol, Godbout, and Gray.[20] This property is caused by the electrostatic repulsion between rigid, negatively charged CNCs that results from the formation of sulfate ester groups during the controlled sulfuric acid hydrolysis of the starting cellulosic material.[21] The repulsion forces between self-organized CNCs are indirectly characterized by the cholesteric pitch, which corresponds to a full helicoid revolution along the chiral nematic axis.[22]

Revol, Godbout, and Gray[23] were the first to report that the self-organization can be preserved by simple evaporation. It results in Bragg reflection of visible light from dried films, with a consequence that iridescence and colored films are obtained only if the pitch length in the solid films is approximately that of the wavelength of visible light.

Since then, there have been several scientific publications, conferences, and patents on this topic, as recently summarized in a book chapter by Abitbol and Cranston.[24] Several physical and chemical parameters are reported to influence the coloration of the iridescence of the film.[25−31] To the best of our knowledge, the most efficient parameters for tuning the film coloration are the addition of monovalent salts and sonication as reported by Beck, Bouchard, and Berry.[29] However, over-sonication or the addition of an excess of salt can irreversibly inhibit the self-organization, resulting in a loss of coloration.

Another outstanding issue is that iridescent films based on only CNC are usually very brittle and difficult to handle. However, only a couple of studies have tried to overcome this drawback. Poly(vinyl alcohol) (PVA) and styrene−butadiene (SB) latex have been used to improve the CNC film flexibility without affecting the iridescence as patented by Zou, Tan, and Berry.[32] More recently, the incorporation of cellulose nanofibrils within the CNC suspension has also been reported to improve film flexibility.[33] In this case, it seems that the iridescent properties of films are inhibited with cellulose nanofibrils addition.

One approach that can address these two issues is to use water-soluble polymers or surfactants to interact with the CNC self-assembly process. In most cases, this promotes the suspension gelation of the CNC suspension, so no chiral nematic order was reported.[34−36] To the best of our knowledge, the use of an anionic polymer for this purpose has never been investigated. Recently, the addition of polyols to the CNC dispersion has been proposed as a means of plasticizing the CNC film,[37] thus eliminating cracking and modifying the coloration of the iridescent films through a redshift.[38]

This study investigates the influence of anionic and neutral water-soluble polymers on the self-assembly properties of CNC in both suspensions and solid films. An anionic polymer, sodium polyacrylate (PAAS), was used to modulate the film's coloration, and a neutral polymer, polyethylene glycol (PEG), was used to improve the film's flexibility. These polymers were selected because they do not cause flocculation of the CNC suspension. The first part of the study determines the main features of CNCs and their self-assembly properties in suspension, and the second part investigates the added polymers' physical and chemical interactions with CNC in suspension.

EXPERIMENTAL SECTION

Materials. The starting material for producing iridescent solid films is a commercial cellulose nanocrystal (CNC) suspension used as received (without dialysis). It was purchased from the UMaine Process Development Center (University of Maine, U.S.A.) that was extracted from wood pulp using sulfuric acid hydrolysis. The dry matter of the CNC suspension was 6.5 wt %, as measured using a moisture analyzer (MA35, Sartorius, Germany).

The anionic sodium polyacrylate (PAAS) is a commercial dispersant agent (TOPSPERCE GXN, Coatex, France). According to the supplier, the molecular weight (M_w) of the dispersant is 5000 g/mol, and the pH is 7.5. The sample is of commercial grade, and so it will have some impurities as received. Poly(ethylene glycol) (PEG) with a molecular weight of 200 g/mol and polyethylenimine (PEI) with a molecular weight of 1300 g/mol were delivered by Sigma-Aldrich (U.S.A.). Deionized water (5 μS/cm) was used in all experiments.

CNC Dispersion. To obtain a homogeneous and well-dispersed suspension, the 6.5 wt % CNC suspension was exposed to a dispersive energy of 5 kJ/g_{CNC} using a 200 W sonication probe (Sonifier S-250A, Branson, U.S.A.). The CNC suspension and 100 μM polymer solutions were mixed with a homogenizer (Ultraturrax T8, IKA, France) for 3 min at room temperature.

Rheological and Self-Assembly Characterizations of CNC Suspensions. The rheological behavior of the suspensions was investigated using a controlled-stress rheometer (Physica MCR 301, Anton Paar Physica, Austria) with a cone/plate spindle (ref no. CC 50) used at a 1 s^{-1} constant shear rate with a 1 mm gap via a Peltier system. Flow curves were recorded at 20 °C for 500 s until flow stabilization, and the viscosity was calculated using the average of the last 30 s. Each measurement was taken in triplicate and averaged.

The texture of the liquid crystal phase was observed using a polarized optical microscope (AXIO Imager M1 m, Carl Zeiss MicroImaging, U.S.A.) in transmission mode. A small drop of the suspension was deposited onto a cavity microslide (L4090, AgarScientific, U.K.) with an 18 mm diameter and a 1.5 mm depth. The chiral-nematic pitch was evaluated by measuring the spacing of the lines in the fingerprint texture. For each microslide, the average pitch was measured at 3 different locations by counting at least 100 lines. The same operating mode was used for the surface analysis of the solid films.

Interactions of the Water-Soluble Polymer with the CNC Suspension. Samples were prepared from CNC suspensions diluted to approximately 0.5 wt % in deionized water or 100 μM polymer solutions (PAAS, PEG, PEI).

The electrophoretic mobility of CNC was measured using a zeta potential analyzer (Zeta2000, Malvern Instruments, U.S.A.). The reported electrophoretic mobility (Ue and zeta potential) was determined from an average of 10 measurements. A few drops of 1 mM NaCl solution was added to maintain the conductivity of the suspension (500 $\mu S \cdot cm^{-1}$).

Dynamic light scattering (DLS) was used to measure the size of the nanoparticles (Vasco I, Corduan Technologies, France). The cumulative method was used, and two parameters were taken into account, the hydrodynamic diameter (z^*) and the polydispersity index (PDI). For each sample, each measurement was replicated 3 times. NaCl solution was added to maintain the conductivity of the suspension (500 $\mu S \cdot cm^{-1}$).

Sorption measurements were taken using a quartz crystal microbalance with dissipation (QCM-D). This instrument (Q-Sense E1, Biolin Scientific, Sweden) measures the resonance frequency of the oscillation of a quartz crystal for its fundamental frequency (5 MHz) and selected overtones (15, 25, 35, 45, 55, and 75 MHz). Only the seventh overtone was used in the data evaluation since it provides both an appropriate measurement sensitivity and very stable and reproducible measurements as compared to lower overtones. The

DOI: 10.1021/am506786t
ACS Appl. Mater. Interfaces 2015, 7, 4010−4018

adsorbed mass (ng/nm^2) was estimated from the frequency change (Δf) using the Sauerbrey equation. Adsorption curves were calculated from the process as carried out onto 100 nm gold-coated quartz crystals (QSX301, Biolin Scientific, Sweden). All measurements were performed under a constant flow rate (100 μL/min) and temperature (23 °C).

Before performing analyses, gold surfaces were cleaned with a "piranha" solution (30% of H_2O_2/NH_3 1:3, by weight) for 20 min at 70 °C, rinsed with deionized water, and then submitted to a UV/ozone treatment (ProCleaner, Bioforce, U.S.A.) for 20 min. Prior to processing, a 100 μM cationic polyethylenimine solution (PEI, Sigma-Aldrich) was adsorbed onto the clean gold surfaces to facilitate the irreversible adsorption and bonding of CNCs to the crystal sensor. In the beginning of each experiment, deionized water was passed through the chamber until a stable baseline (Δf < 0.05/min) was achieved for 5−20 min.

Solid Film Formation. CNC suspensions (at 5.3 wt % with or without PEG and PAAS) were cast (5 mL per film) into a smooth aluminum plate (6 cm in diameter) and left to dry for 3 days under ambient and controlled conditions (50% RH, 23 °C). For each series, 4 dry free-standing films of 100 g/m^2 were obtained and stored under these conditions until analysis.

Film Characterization. The structural coloration of the films was analyzed using UV−visible spectroscopy (UV 1800, Shimadzu, Japan). The absorption intensity of the solid film was recorded within the wavelength range of 200 to 1100 nm with a normal incidence. For each film, 3 different measurements and 10 scans were recorded and averaged.

Mechanical properties were measured using a universal testing machine (Model 4465, Instron Engineering Corporation, U.S.A.). Young's modulus, the tensile strength, and the elongation rate were established following the ISO-1924-2:2008 standard. For each series, six samples of 15 mm in width and 50 mm in length were submitted to a 10 mm/min constant rate of elongation.

The thermal degradation of the samples was monitored using TGA (thermogravimetric analyzer, STA 6000, PerkinElmer Instruments, U.K.). The mass loss was recorded for a 30 mg subsample upon a heating rate of 10 °C/min in the temperature range of 30−950 °C under an oxidizing atmosphere (air). The analyses were duplicated and averaged.

FE-SEM (field-emission scanning electron microscopy) was used to observe the film microstructure (Ultra 55 ©, Zeiss, Germany). Samples were glued onto a specific holder and coated with a 2 nm layer of gold/palladium to ensure the conductivity of all samples. The accelerating voltage (EHT) was 3 kV for a working distance of 6.4 mm.

RESULTS AND DISCUSSION

Self-Assembly Property of CNCs in Suspension. Before proceeding to the film formation, the physical and chemical properties of the commercial cellulose nanocrystal (CNC) suspension were determined as summarized in Supporting Information Table SI-1. CNCs have a rod-like shape (Supporting Information Figure SI-1), and their average dimensions are 5 nm thick by 205 nm long. Such a morphology is in accordance with previous studies for CNCs extracted with similar hydrolysis conditions (wood pulp and sulfuric acid).[13] The XRD pattern (Supporting Information Figure SI-2) is typical of the crystalline polymorph of neat cellulose I (native cellulose). The major crystalline peak (002) occurs at 22.84°, and the associated crystallinity index (CI) is 88%. The sulfur content estimated via ICP-AES elemental analysis is 370 μmol/g_{CNC}. The surface charge density is approximately 0.56 e/nm^2, as calculated using both AFM and EA. By comparison, values between 0.16 and 0.66 e/nm^2 were previously reported for CNCs having self-assembly properties.[25,26] Therefore, according to these preliminary characterizations, it should be possible to obtain colored films from this pilot-scale production of CNCs.

As mentioned in the introduction, it is essential to determine the critical anisotropic concentration C_A^* for which the suspension is completely anisotropic.[39] For this purpose, rheological analyses as a function of the CNC concentration were combined with polarized optical microscopy (POM), as illustrated in Figure 1.

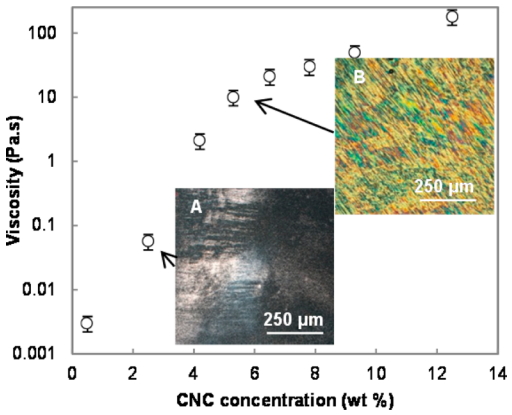

Figure 1. Viscosity as a function of the CNC concentration (25 °C with a shear of 1/s) with the corresponding micrographs between crossed polarizers (A: 2.5 wt % and B: 5.3 wt %).

A well-dispersed CNC suspension of 13 wt % concentration was prepared by centrifugation (10 000 × g, 10 min, 10 °C). Other concentrations were prepared with successive dilutions to a minimum of 0.5 wt % using DI water and sonicated at 5 kJ/g_{CNC}. The minimal concentration in which an anisotropic texture was observed was approximately 2.5 wt % (Figure 1A). Below this concentration, the suspension was isotropic, with CNC randomly dispersed in the aqueous medium. At 5.3 wt %, the CNC suspension was predominantly anisotropic, and fingerprint textures were observed on the whole POM micrograph (Figure 1B). The value of C_A^* reported here is in accordance with a more extensive study in which the authors reported a value of 6.5 wt % obtained with the study of phase separation of CNC isolated from cotton filter with a surface charge density of 0.35 e/nm^2.[40] A concentration of 5.3 wt % has been considered as the optimum concentration for casting CNC suspensions to manufacture iridescent solid films considering the suspension is both predominantly anisotropic and not too viscous to obtain a good film by evaporation.

Interactions of Water-Soluble Polymers with the CNC Suspension. Before discussing the manufacturing of iridescent CNC films, this section focuses on the interactions of anionic or neutral polymers with CNC in suspension. Two polymers have been investigated, an anionic dispersant, i.e., sodium polyacrylate (PAAS), to tune the coloration of the iridescent CNC film and a neutral plasticizer, i.e., polyethylene glycol (PEG), to improve film flexibility. In addition, a classic cationic polymer, polyethylenimine (PEI), was also tested to understand the interactions that favor deposition onto CNCs, as measured by QCM-D.

It is assumed that a colloidal dispersion is stabilized via either electrostatic repulsion or steric stabilization with adsorbed or grafted polymers.[41] One advantage of CNC stabilized via steric stabilization is that the colloidal state is less sensitive to the presence of monovalent salt.[42] In the other cases, phys-

DOI: 10.1021/am506786t
ACS Appl. Mater. Interfaces 2015, 7, 4010−4018

Table 1. Electrokinetic Potential, Hydrodynamic Size, and Colloidal Behavior of a 0.5 wt % CNC Suspension Dispersed in Water and 100 μM Water-Soluble Polymer Solutions[a]

		CNC dispersed in			
		DI water	PAAS	PEG	PEI
apparent hydrodynamic radius[a]	z^* (nm)	105 (5)	102 (10)	122 (10)	856 (8)
	PDI	0.20 (0.05)	0.18 (0.05)	0.22 (0.08)	0.75 (0.22)
electrokinetic potential[c]	pζ (mV)	−44.8 (1.2)	−45.3 (0.8)	−32.3 (1.0)	+15.0 (1.1)
	Ue (V)	−3.5 (0.07)	−3.5 (0.2)	−3.22 (0.09)	1.18 (0.09)
colloidal behavior[d]		birefringent	birefringent	birefringent	no

[a]Values in brackets refer to the standard deviations. [b]Obtained via DLS analyses. [c]Obtained via zeta potential analyses. [d]Observation between cross polar after stirring.

icochemical interactions are critical to iridescence because the self-assembly of CNCs is extremely sensitive to the electrochemical equilibrium.[27] The *zeta* potential can be used as a measurement of the electrostatic repulsive forces, which can provide information on the stability of the colloidal system and indirectly on the self-organization of CNCs in suspension. A value smaller than ±15 mV is considered to indicate the onset of particle agglomeration. Values greater than ±30 mV generally mean that there is sufficient mutual repulsion, which results in colloidal stability.[43]

Table 1 compares the hydrodynamic and electrokinetic parameters of CNCs dispersed in deionized water with ionic (PAAS) and nonionic (PEG) polymers. The zeta potential of CNCs dispersed in deionized water is highly negative (−44.5 mV) due to the high surface charge density of the sulfate half-ester groups.

In the presence of anionic polymers such as PAAS, the surface charge remains highly negative (−45.3 mV) and the hydrodynamic diameter is unmodified. Upon the addition of a neutral polymer like PEG, the mobility decreases (−32.3 mV) because of polymer absorption. It also influences the hydrodynamic diameter (z*), which increases from 105 to 122 nm. As for CNCs dispersed in DI water, intense birefringence patterns are observed for CNCs dispersed in PAAS and PEG solutions (Supporting Information Figure SI-3). This confirms the absence of agglomeration, as well as the preservation of the self-assembly properties of CNC in suspension. In contrast, in the case of dispersion in a cationic PEI solution, the flow birefringence completely disappeared (Supporting Information Figure SI-3) and the zeta potential shifted from −44.5 mV to +15.0 mV. This confirms an ionic interaction between the negative sulfate half-ester groups of CNCs and the positive amino groups of PEI. This also led to the formation of particle flocculation, as proven via DLS measurement (z^* = 856 nm). This last experiment was conducted only to evaluate the absorption phenomena because PEI was only used for the functionalization of the gold-coated mica plate for QCM experiments and CNC deposition.

Adsorption Phenomena of the Water-Soluble Polymer with CNC. The adsorption phenomena were evaluated using a quartz crystal microbalance (QCM) (Figure 2) in combination with AFM analysis (Figure 3).

As a preliminary investigation, it was verified that the absorbed CNC layer was thick enough to avoid a positively charged substrate effect with PEI. On the basis of the frequency drop ($\Delta f \sim -57$ Hz) and the Sauerbrey equation, the average adsorbed weight of CNC onto the substrate was approximately 1180 ng/cm^2, corresponding to a CNC layer of approximately 7 nm, assuming the density of CNCs is 1.53. This confirms that the adsorbed CNC layer is thick enough to avoid possible interactions with the cationically charged sensor (PEI layer).

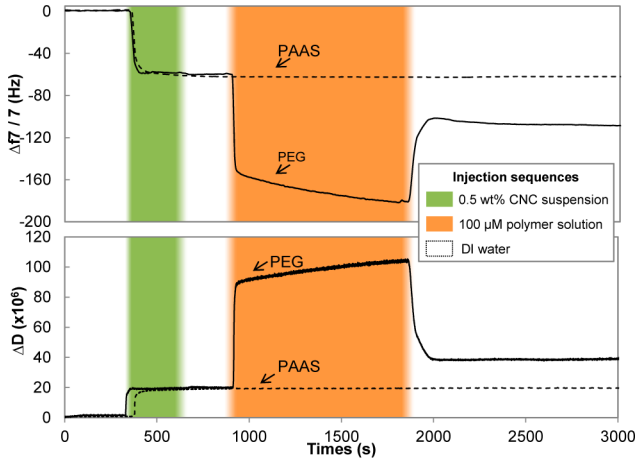

Figure 2. QCM-D studies (seventh overtone) of CNC and polymer (PAAS and PEG) adsorption on a PEI-modified gold surface. The first injection corresponds to the 0.5 wt % CNC suspension (green area) whereas the second injection corresponds to the 100 μM polymer solutions (orange area). Uncolored sections correspond to the rinsing stage with DI water.

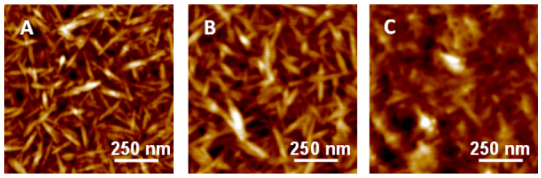

Figure 3. AFM pictures (height sensor) corresponding to the air-dried substrate analysis of QCM experiments: after injection of CNC and rinsing (A), after injection of PAAS and rinsing (B), and after injection of PEG and rinsing (C).

AFM analyses were carried out on the air-dried substrate surface after CNC adsorption and rinsing with DI water (Figure 3A). These AFM pictures emphasize that the CNC adsorbed layer displays good surface coverage with a random orientation of rods. The CNC layer can also form a three-dimensional network with a larger exposed surface area. The adsorbed CNC cannot be considered as a continuous layer, as can films formed by classical polymers with a high film-forming ability. Hence, for further calculation of the amount of adsorbed polymers on the CNC substrate, it is necessary to take into consideration the specific surface topography of the CNC layer as proposed for CNFs by Ahola, Salmi, Johansson, Laine, and Österberg.[44] From AFM calculations carried out on three scanning areas of 9 μm^2, the developed surface area of the CNC layer is

DOI: 10.1021/am506786t
ACS Appl. Mater. Interfaces 2015, 7, 4010−4018

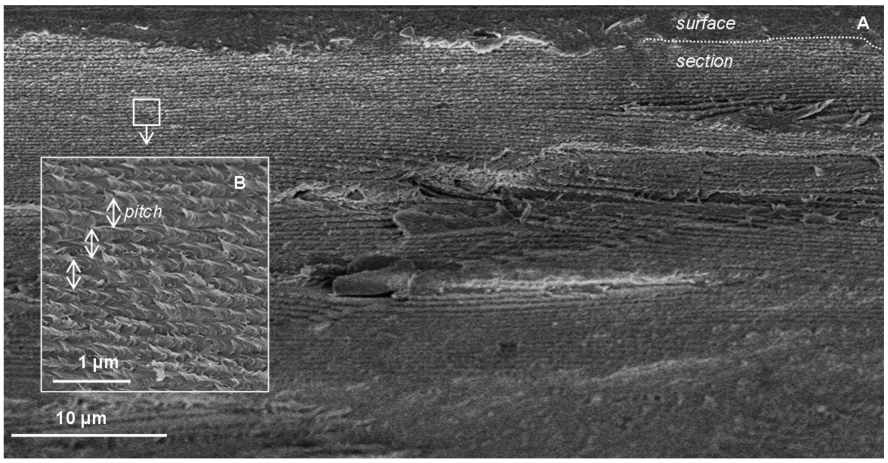

Figure 4. FE-SEM images of a fracture surface across an iridescent CNC film.

approximately 16 ± 2 μm^2. This means that, for an adsorption study using QCM, a sensor of 1 cm^2 must be considered to have a surface area of 1.8 cm^2. On the basis of the heterogeneity of the CNC substrate, the amount of adsorbed polymer should be considered only semiquantitative.

When PAAS is injected, no adsorption ($\Delta f < -0.5$ Hz) was detected using QCM. That makes sense because PAAS as an anionic surfactant has no tendency to adsorb onto negatively charged CNCs.

Furthermore, there is no difference between AFM images before and after the injection of PAAS (Figure 3A,B), confirming the absence of adsorption of PAAS onto CNC, suggesting depletion stabilization.

On the other hand, QCM measurements upon the adsorption of PEG show a large frequency drop ($\Delta f \sim -121$ Hz), suggesting the occurrence of physical sorption. For this polymer, nonionic interactions (hydrogen bonds) between CNCs and PEG may be the cause of the sorption phenomena. Just after the injection of PEG solution, an important desorption ($\Delta f \sim +79$ Hz) is observed during rinsing with DI water. This confirms that CNC surfaces are saturated with the adsorbed polymer, suggesting steric stabilization. The absorbed amount of PEG on the CNC surface ($\Delta f \sim -40$ Hz, i.e., 830 ng/cm^2) is equivalent to that reported by Hu, Cranston, Ng, and Pelton[36]for hydroxylpropyl guar (HPG) on similar surfaces.

Using the average CNC dimensions (5 nm × 5 nm × 205 nm), the specific surface area is calculated to be 250 m^2/g, and the adsorption of PEG can be estimated to be 580/g_{CNC}, i.e., 12 wt %. AFM (Figure 3C) highlights that, after PEG adsorption onto the CNC substrate, the layer appears to be smoother, suggesting that polymer coating onto the CNCs has indeed occurred. By comparison with other studies, when PEG is covalently grafted onto desulfated CNC[45] or carboxylated CNC,[46] the adsorption is significantly higher, approximately 1−1.5 mmol/g_{CNC}.

To summarize, neutral PEG can be physically adsorbed onto CNCs and, due to steric stabilization and nonionic interactions (hydrogen bonds), the self-assembly of the suspension is retained as previously reported with PEG-grafted CNCs.[45] Limited interactions were found to originate from the adsorption of anionic PAAS, as expected, and the CNCs maintained their self-assembly properties due to depletion stabilization (i.e., free polymer in the dispersion medium). Next, we will evaluate the influence of these polymers on the final CNC iridescent solid film.

Adsorption Phenomena of the Water-Soluble Polymer with CNC. Following the simple evaporation of the CNC suspension, the self-assembly properties are preserved within the solid films, which results in their structural organization as shown in Figure 4. Similar FE-SEM observations were recently reported by Majoinen, Kontturi, Ikkala, and Gray.[47]

At low magnification, FE-SEM analyses (Figure 4A) indicate that the layers remain parallel to each other. In contrast, Figure 4B gives an interesting indication of the pitch length and the preferential orientation of CNCs (handedness and direction). The self-assembly of CNCs has also an impact at different scales and not only on the film coloration. For instance, barrier and mechanical properties are different when comparing a structured film to a nonordered film made from the same CNC suspension.[48] In comparison to a nonordered film, the mechanical properties for a structural film are low, and generally the iridescent film is very brittle with a high Young's Modulus and a low strain at break.[48]

Tuning of Iridescent Solid Film Coloration. Adjusting the coloration by modifying the chiral-nematic organization and improving the color homogeneity is essential for developing an optical material for anticounterfeit applications. One effective parameter is the sonication process, which leads to a solid film redshift,[29] and the addition of monovalent salt (NaCl), which causes a blueshift to the solid film.[49] However, several limitations exist when monovalent salt is added, namely, (i) an irreversible inhibiting effect on self-organization, (ii) tuning coloration with NaCl being limited to a specific range of ionic strengths, and (iii) an excess of salt (concentrations greater than 20 mM)[48] causing particle agglomeration and suspension gelation. To overcome these issues, neither salt nor cationic polymer was used in this study. Instead the anionic linear polyelectrolyte PAAS with a low molecular weight ($M_W \sim 5000$ g/mol) has been used for tuning coloration. In contrast to monovalent salt, the high density of negative groups (COO−) prevent PAAS from adsorbing with the CNC, as confirmed using QCM-D (Figure 2) and electrokinetic potential analysis (Table 1). At the macroscale, though, the addition of PAAS modifies the rheology and chiral nematic organization of the CNC suspension. Figure 5 presents the evolution of the suspension viscosity as a function of the PAAS concentration.

Upon adding PAAS, the viscosity sharply decreased, reaching a minimum of 4.1 Pa·s at 160 μmol/g_{CNC} of PAAS. A higher

DOI: 10.1021/am506786t
ACS Appl. Mater. Interfaces 2015, 7, 4010−4018

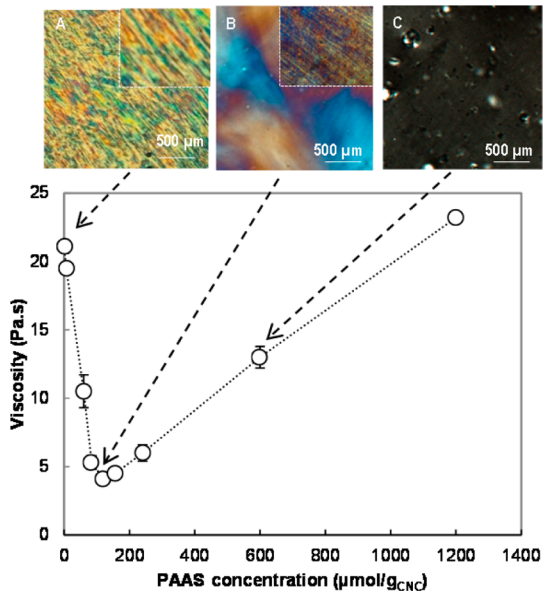

Figure 5. Viscosity of a 5.3 wt % CNC suspension as a function of the PAAS concentration (at 25 °C for a shear of 1 Hz), accompanied by fingerprint textures (A, B, and C), as observed using polarized optical microscopy.

amount of PAAS results in the inhibition of the self-organization of the films, as detected by the disappearance of the fingerprint texture when using higher PAAS concentration than 600 μmol/gCNC.

It has been shown in the previous section that there is no adsorption of PAAS with CNC, suggesting depletion stabilization. Even with their small size ($R_{gyration}$ ≈ 3.4 nm), anionic polymer chains will have no tendency to interleave between negatively charged CNCs. PAAS is more likely to move outside crystallites in which electrostatic repulsion will not be predominant. This will lead to a nonhomogenous repartition of PAAS within the CNC suspension, leading to a concentration difference around and within crystallites. This concentration difference of PAAS creates an osmotic pressure difference, resulting in a decrease of both chiral nematic pitch and viscosity as illustrated in Scheme 1. Such statement must be assessed by small angel X-ray diffraction (SAXD) experiments at the nanoscale.[50]

Another explanation could be the highly hygroscopic behavior of PAAS, which is able to absorb water up to 100 times its initial weight.[51] Moreover, it has been reported by Zhang, Chodavarapu, Kirk, and Andrews[52] that water sorption

Scheme 1. Mechanism That Could Explain the Blueshift Occurring upon the Addition of PAAS

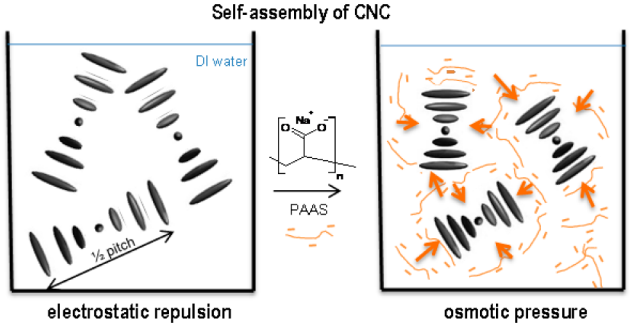

within CNC iridescent films has caused a redshift. Thus, it can be assumed that the remaining free water molecules may be predominantly absorbed by PAAS, explaining the decrease in pitch in the CNC film.

The analyses were then carried out in the solid state by measuring the maximal absorption wavelength (λ_{max}) and the fingerprint pitch of films, as shown in Figure 6A. The addition of PAAS in increasing amounts (ranging from 0 to 160 μmol/g) causes a blueshift of solid films without affecting the color intensity as measured by UV−visible absorption measurement at normal incidence (see Supporting Information Figure SI-4).

As shown in Figure 6A, the neat CNC film absorbs in near-infrared wavelengths with a λ_{max} at 1006 nm. This results in the absence of coloration in visible wavelengths. In this case, the absence of coloration is explained by the high dispersive energy applied to the CNC suspension (5 kJ/g). A strong sonication treatment is applied to the initial CNC suspension to cover a wide range of coloration with the addition of PAAS. The preservation of the self-assembly at the solid state in neat CNC films is also revealed by the presence of the fingerprint texture observed using polarized optical microscopy (Figure 6C). With the addition of an optimal range of PAAS (120−160 μmol/g), solid films displayed an intense green coloration (Figure 6B) with a much narrower absorption peak (Supporting Information Figure SI-4). Lastly, fingerprint textures are more regular and better pronounced,

To summarize, an anionic linear polymer such as PAAS can be used for tuning the coloration within CNC films. For instance, the addition of approximately 160 μmol/g_{CNC} of PAAS results in a green coloration (λ_{max} = 600 nm) and a well-pronounced fingerprint texture.

Improvement of CNC Solid Film Flexibility Using PEG. Even if the coloration of the iridescent CNC film can be finely tuned using PAAS, such films are very brittle, which limits the industrial application of these emerging photonic materials as laminate films or surface coatings. To improve their flexibility and reduce material consumption and cost, PEG was used as a plasticizer of the iridescent solid films. The preservation of their self-organization is expected due to the steric repulsion and nonionic interaction demonstrated in the previous section. The ratio between PEG and CNC in the prepared films was limited to the equivalent amount previously determined using QCM experiments, approximately 0.6 mmol/g_{CNC} (12 wt %). As presented in Table 2, the coloration in the CNC films were maintained, resulting in iridescent properties similar to those of the CNC film obtained without plasticizer (Film A). The preservation of iridescent properties was also reported when PVOH was added to CNC.[31] A moderate redshift was noted, with the coloration (λ_{max}) shifting from 595 to 623 nm, upon the addition of 10 wt % PEG. However, this redshift is much less pronounced than that obtained upon the use of glucose as a plasticizer.[38] Two reasons may explain the relatively small effect of PEG on CNC self-assembly into solid films. First, the low molecular weight (200 g/mol, i.e., DP ≈ 5) of the polymer favors polymer chain mobility and avoids bridging flocculation. Second, nonionic interactions with CNC preferentially induce steric stabilization.

The mechanical properties decreased with increasing amounts of PEG because of its plasticizing effect. A decrease in the force at break of 45%, a decrease in the Young's Modulus of 55%, and a more than doubling of the strain at break were observed when comparing the reference film (Film A) to a film incorporating 10 wt % PEG (Film D). As a consequence, a

DOI: 10.1021/am506786t
ACS Appl. Mater. Interfaces 2015, 7, 4010−4018

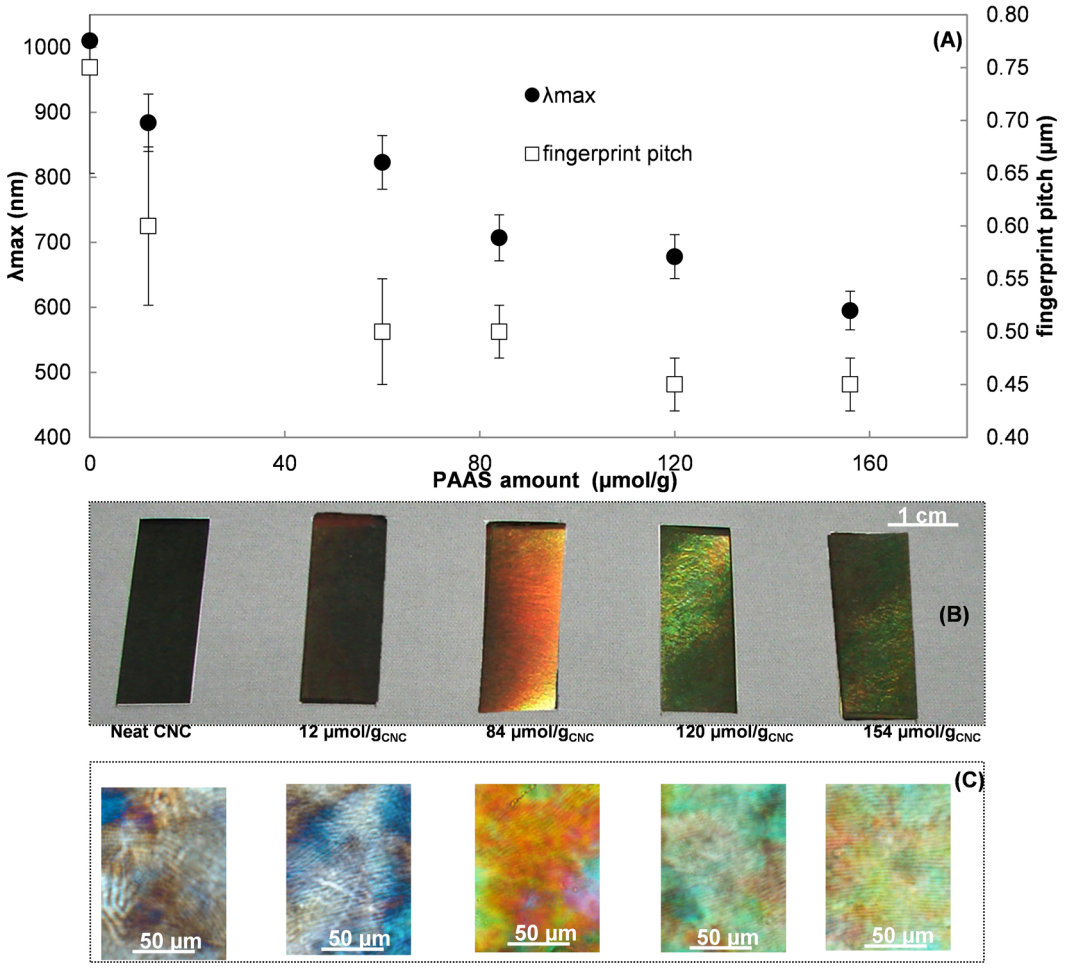

Figure 6. Evolution of the maximum absorption wavelength (λ_{max}) (●) and average fingerprint pitch (□), as a function of PAAS ratios in 100 g/m^2 CNC films (A). Observation under natural light on a black background of corresponding iridescent CNC films (B), accompanied by the optical microscope image (cross-polarized light) of the film surface (C).

Table 2. Comparison of Optical and Mechanical Properties of 100 g/m^2 Films Produced from the Same CNC Suspension Containing Amounts of PEG[a]

		Film A (control)	Film B	Film C	Film D
contexture	PEG to CNC ratio (wt %)	-	2.5	5.0	10.0
	grammage (g/m^2)	96 (2)	97 (3)	103(3)	98 (5)
	thickness (μm)	72 (1)	71 (3)	80 (3)	79 (1)
	density	1.33 (0.06)	1.35 (0.10)	1.28 (0.02)	1.24 (0.08)
optical properties	λ_{max} (nm)	595 (13)	585 (25)	615 (5)	623 (25)
mechanical properties	elongation at break (%)	0.70 (0.1)	1.1 (0.3)	1.80(0.5)	1.70(0.3)
	force at break (MPa)	35 (7)	30 (3)	29 (7)	19 (9)
	specific Young's modulus (GPa)	5.8 (1.0)	4.5 (0.3)	2.6 (1.3)	2.4 (1.5)

[a]Values in brackets refer to the standard deviations.

flexible and intensely iridescent film is obtained, as presented in Figure 7.

When comparing this film with one reinforced with cellulose nanofibers,[33] the mechanical properties (Young's modulus, force at break and strain at break) are very similar. However, a moderate iridescence property is observed with the addition of 1 wt % of cellulose nanofibers (CNFs), which allowed preserving the self-assembly of CNC using much less "plasticizer". Thus, a 10 times lower amount of CNF gave similar results as those reached using PEG. With a cost-efficient approach, one of the benefits of using PEG is to save expensive CNC[53] (ca. $50 to $200 per kg) in self-assembly films while having almost the same optical properties than with a neat CNC film. As revealed with thermal analysis (Figure 8), another benefit of the use of PEG is that it thermally insulates the CNC, increasing its thermal stability.

The excellent compatibility between PEG and CNC results in an increase of the onset of thermal temperature degradation by 35 °C when comparing neat CNC (T_{deg} = 203 °C) with a film incorporating 10 wt % of PEG (T_{deg} = 238 °C).

Similar results were reported by Ben Azouz, Ramires, Van den Fonteyne, El Kissi, and Dufresne[54] for noniridescent CNC used as reinforcement in extruded composites with higher molecular weight (M_w = 5 × 10^6 g/mol) PEO. It is worth

DOI: 10.1021/am506786t
ACS Appl. Mater. Interfaces 2015, 7, 4010−4018

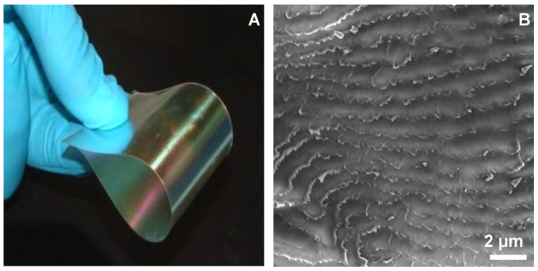

Figure 7. 98 g/m^2 iridescent CNC film plasticized with 10 wt % PEG (A) and the corresponding film cross-section observed by FE-SEM (B).

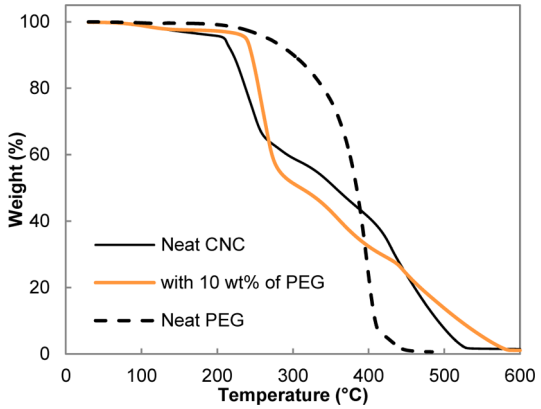

Figure 8. Comparison of TG curves of neat CNC and CNC with 10 wt % of PEG.

noting the advantage of a superior heat resistance in extrusion or lamination treatments. The procedure used in our study is simple to operate, providing a clear advantage in the preparation of flexible and strong iridescent CNC-based films.

CONCLUSION

To improve the flexibility and to modulate the coloration of iridescent CNC films, this study investigated the influence of two water-soluble polymers on the self-assembly properties of the suspension of these particles and on the solid film. An anionic polymer, sodium polyacrylate (PAAS) was used to modulate the film coloration, and a neutral polymer, polyethylene glycol (PEG), was used to improve the iridescent film flexibility. The average dimensions of CNC used in this study were 5 nm thick by 205 nm long with a surface charge density of 0.56 e/nm^2. At 5.3 wt %, the CNC suspension is completely anisotropic, and a fingerprint texture was observed. The neutral PEG can be physically adsorbed onto CNC and, due to steric stabilization and nonionic interactions (hydrogen bonds), the self-assembly of the suspended CNC was conserved. Upon the addition of anionic PAAS, limited interactions were observed and the CNC maintained its self-assembly properties. As a key result, the addition of 10 wt % makes films much more flexible (with double the elongation: 1.8 instead of 0.7%) while preserving the coloration and increasing the degradation temperature by almost 35 °C. PAAS can be used for tuning the coloration within CNC films. It causes a stronger, narrower coloration in the visible spectrum (higher absorption) with a well-pronounced fingerprint texture. For instance, the addition of approximately 160 μmol/g$_{CNC}$ of PAAS results in an intense green coloration (λ_{max} = 600 nm). Such results open up the prospect of biobased materials dedicated to decorative, security, and anticounterfeit flexible films following a biomimetic approach.

ASSOCIATED CONTENT

Supporting Information

Morphological and chemical characterization of CNC in Table S1, AFM pictures of individualized CNCs in Figure S1, XRD pattern of neat CNC in Figure S2, crossed polarizers observation of 0.5 wt % CNC dispersed in water (A) and in 100 μM polymers solutions of PAAS (B), PEG (C), and PEI in Figure S3, and absorption spectrum of CNC films with increasing amounts of PAAS in Figure 4. This material is available free of charge via the Internet at http://pubs.acs.org.

AUTHOR INFORMATION

Corresponding Author

*E-mail: julien.bras@grenoble-inp.fr.

Notes

The authors declare no competing financial interest.

ACKNOWLEDGMENTS

The authors gratefully acknowledge Papeteries du Léman and the French National Research Agency (ANRT) for the financial and material support for the Ph.D. thesis. TekLiCell cluster and Region Rhone-Alpes are acknowledged for their financial support of the experimental setups. We would like to thank Francine Roussel (Grenoble Institute of Technology) for her expertise in providing SEM imaging and Stéphane Coindeau for undertaking the XRD analysis. LGP2 is part of LabEx Tec 21 (Investissements d'Avenir - grant agreement no. ANR-11-LABX-0030) and of the Energies du Futur and PolyNat Carnot Institutes.

REFERENCES

(1) Kinoshita, S.; Yoshioka, S.; Miyazaki, J. Physics of Structural Colors. *Rep. Prog. Phys.* **2008**, *71*, 076401.
(2) Meadows, M. G.; Butler, M. W.; Morehouse, N. I.; Taylor, L. A.; Toomey, M. B.; McGraw, K. J.; Rutowski, R. L. Iridescence: Views from Many Angles. *J. R. Soc., Interface* **2009**, *6*, S107−S113.
(3) Kinoshita, S.; Yoshioka, S. Structural Colors in Nature: The Role of Regularity and Irregularity in the Structure. *ChemPhysChem* **2005**, *6*, 1442−1459.
(4) Doucet, S. M.; Meadows, M. G. Iridescence: A Functional Perspective. *J. R. Soc., Interface* **2009**, *6*, S115−S132.
(5) Vignolini, S.; Rudall, P. J.; Rowland, A. V.; Reed, A.; Moyroud, E.; Faden, R. B.; Baumberg, J. J.; Glover, B. J.; Steiner, U. Pointillist Structural Color in Pollia Fruit. *Proc. Natl. Acad. Sci. U. S. A.* **2012**, *109*, 15712−15715.
(6) Whitney, H. M.; Kolle, M.; Andrew, P.; Chittka, L.; Steiner, U.; Glover, B. J. Floral Iridescence, Produced by Diffractive Optics, Acts as a Cue for Animal Pollinators. *Science* **2009**, *323*, 130−133.
(7) Glover, B. J.; Whitney, H. M. Structural Colour and Iridescence in Plants: The Poorly Studied Relations of Pigment Colour. *Ann. Bot.* **2010**, *105*, 505−511.
(8) Parker, A. R.; Townley, H. E. Biomimetics of Photonic Nanostructures. *Nat. Nanotechnol.* **2007**, *2*, 347−353.
(9) Moon, R. J.; Martini, A.; Nairn, J.; Simonsen, J.; Youngblood, J. Cellulose Nanomaterials Review: Structure, Properties and Nanocomposites. *Chem. Soc. Rev.* **2011**, *40*, 3941−3994.
(10) Shopsowitz, K. E.; Hamad, W. Y.; MacLachlan, M. J. Flexible and Iridescent Chiral Nematic Mesoporous Organosilica Films. *J. Am. Chem. Soc.* **2011**, *134*, 867−870.
(11) Lagerwall, J. P. F.; Schutz, C.; Salajkova, M.; Noh, J.; Hyun Park, J.; Scalia, G.; Bergstrom, L. Cellulose Nanocrystal-Based Materials:

DOI: 10.1021/am506786t
ACS Appl. Mater. Interfaces 2015, 7, 4010−4018

From Liquid Crystal Self-Assembly and Glass Formation to Multifunctional Thin Films. *NPG Asia Mater.* **2014**, *6*, e80.
(12) Charreau, H.; Foresti, M.; Vazquez, A. Nanocellulose Patents Trends: A Comprehensive Review on Patents on Cellulose Nanocrystals, Microfibrillated and Bacterial Cellulose. *Recent Pat. Nanotechnol.* **2013**, *7*, 56−80.
(13) Habibi, Y.; Lucia, L. A.; Rojas, O. J. Cellulose Nanocrystals: Chemistry, Self-Assembly, and Applications. *Chem. Rev.* **2010**, *110*, 3479−3500.
(14) Dufresne, A. *Nanocellulose, from Nature to High Performance Tailored Materials*; De Gruyter: Berlin, Germany, 2012.
(15) Eichhorn, S. J.; Dufresne, A.; Aranguren, M.; Marcovich, N. E.; Capadona, J. R.; Rowan, S. J.; Weder, C.; Thielemans, W.; Roman, M.; Renneckar, S.; Gindl, W.; Veigel, S.; Keckes, J.; Yano, H.; Abe, K.; Nogi, M.; Nakagaito, A. N.; Mangalam, A.; Simonsen, J.; Benight, A. S.; Bismarck, A.; Berglund, L. A.; Peijs, T. Review: Current International Research into Cellulose Nanofibres and Nanocomposites. *J. Mater. Sci.* **2010**, *45*, 1−33.
(16) Peng, B. L.; Dhar, N.; Liu, H. L.; Tam, K. C. Chemistry and Applications of Nanocrystalline Cellulose and Its Derivatives: A Nanotechnology Perspective. *Can. J. Chem. Eng.* **2011**, *89*, 1191−1206.
(17) Lin, N.; Huang, J.; Dufresne, A. Preparation, Properties and Applications of Polysaccharide Nanocrystals in Advanced Functional Nanomaterials: A Review. *Nanoscale* **2012**, *4*, 3274−3294.
(18) Tingaut, P.; Zimmermann, T.; Sèbe, G. Cellulose Nanocrystals and Microfibrillated Cellulose as Building Blocks for the Design of Hierarchical Functional Materials. *J. Mater. Chem.* **2012**, *22*, 20105−20111.
(19) Gray, D. G. Chiral Nematic Ordering of Polysaccharides. *Carbohydr. Polym.* **1994**, *25*, 277−284.
(20) Revol, J.-F.; Godbout, J. D. L.; Gray, D. G. *Solidified Liquid Crystals of Cellulose with Optically Variable Properties*. WO9521901A1, 1995.
(21) Marchessault, R. H.; Morehead, F. F.; Walter, N. M. Liquid Crystal Systems from Fibrillar Polysaccharides. *Nature* **1959**, *184*, 632−633.
(22) de Vries, H. I. Rotatory Power and Other Optical Properties of Certain Liquid Crystals. *Acta Crystallogr.* **1951**, *4*, 219−226.
(23) Revol, J.-F.; Godbout, L.; Gray, D. Solid Self-Assembled Films of Cellulose with Chiral Nematic Order and Optically Variable Properties. *J. Pulp Pap. Sci.* **1998**, *24*, 146−149.
(24) Abitbol, T.; Cranston, E. D. Chiral Nematic Self-Assembly of Cellulose Nanocrystals in Suspensions and Solid Films. *Handbook of Green Materials*; World Scientific: 2014; Chapter 4, pp 37−56.
(25) Beck, S.; Roman, M.; Gray, D. G. Effect of Reaction Conditions on the Properties and Behavior of Wood Cellulose Nanocrystal Suspensions. *Biomacromolecules* **2005**, *6*, 1048−1054.
(26) Dong, X. M.; Revol, J.-F.; Gray, D. G. Effect of Microcrystallite Preparation Conditions on the Formation of Colloid Crystals of Cellulose. *Cellulose* **1998**, *5*, 19−32.
(27) Araki, J.; Kuga, S. Effect of Trace Electrolyte on Liquid Crystal Type of Cellulose Microcrystals. *Langmuir* **2001**, *17*, 4493−4496.
(28) Pan, J.; Hamad, W.; Straus, S. K. Parameters Affecting the Chiral Nematic Phase of Nanocrystalline Cellulose Films. *Macromolecules* **2010**, *43*, 3851−3858.
(29) Beck, S.; Bouchard, J.; Berry, R. Controlling the Reflection Wavelength of Iridescent Solid Films of Nanocrystalline Cellulose. *Biomacromolecules* **2011**, *12*, 167−172.
(30) Nguyen, T.-D.; Hamad, W. Y.; MacLachlan, M. J. Tuning the Iridescence of Chiral Nematic Cellulose Nanocrystals and Mesoporous Silica Films by Substrate Variation. *Chem. Commun.* **2013**, *49*, 11296−11298.
(31) Beck, S.; Bouchard, J.; Chauve, G.; Berry, R. Controlled Production of Patterns in Iridescent Solid Films of Cellulose Nanocrystals. *Cellulose* **2013**, *20*, 1401−1411.
(32) Zou, X.; Tan, X.; Berry, R. *Flexible, Iridescent Nanocrystalline Cellulose Film, and Method for Preparation*. WO2010124378A1, 2010.
(33) Xiong, R.; Han, Y.; Wang, Y.; Zhang, W.; Zhang, X.; Lu, C. Flexible, Highly Transparent and Iridescent All-Cellulose Hybrid Nanopaper with Enhanced Mechanical Strength and Writable Surface. *Carbohydr. Polym.* **2014**, *113*, 264−271.
(34) Dorris, A.; Gray, D. Gelation of Cellulose Nanocrystal Suspensions in Glycerol. *Cellulose* **2012**, *19*, 687−694.
(35) Boluk, Y.; Zhao, L.; Incani, V. Dispersions of Nanocrystalline Cellulose in Aqueous Polymer Solutions: Structure Formation of Colloidal Rods. *Langmuir* **2012**, *28*, 6114−6123.
(36) Hu, Z.; Cranston, E. D.; Ng, R.; Pelton, R. Tuning Cellulose Nanocrystal Gelation with Polysaccharides and Surfactants. *Langmuir* **2014**, *30*, 2684−2692.
(37) Kelly, J. A.; Yu, M.; Hamad, W. Y.; MacLachlan, M. J. Large, Crack-Free Freestanding Films with Chiral Nematic Structures. *Adv. Opt. Mater.* **2013**, *1*, 295−299.
(38) Mu, X.; Gray, D. G. Formation of Chiral Nematic Films from Cellulose Nanocrystal Suspensions Is a Two-Stage Process. *Langmuir* **2014**, *30*, 9256−9260.
(39) Shafiei-Sabet, S.; Hamad, W. Y.; Hatzikiriakos, S. G. Rheology of Nanocrystalline Cellulose Aqueous Suspensions. *Langmuir* **2012**, *28*, 17124−17133.
(40) Ureña-Benavides, E. E.; Ao, G.; Davis, V. A.; Kitchens, C. L. Rheology and Phase Behavior of Lyotropic Cellulose Nanocrystal Suspensions. *Macromolecules* **2011**, *44*, 8990−8998.
(41) Hu, Z.; Cranston, E. D.; Ng, R.; Pelton, R. Tuning Cellulose Nanocrystal Gelation with Polysaccharides and Surfactants. *Langmuir* **2014**, *30*, 2684−2692.
(42) Araki, J.; Wada, M.; Kuga, S. Steric Stabilization of a Cellulose Microcrystal Suspension by Poly(Ethylene Glycol) Grafting. *Langmuir* **2000**, *17*, 21−27.
(43) Mirhosseini, H.; Tan, C. P.; Hamid, N. S. A.; Yusof, S. Effect of Arabic Gum, Xanthan Gum and Orange Oil Contents on Z-Potential, Conductivity, Stability, Size Index and Ph of Orange Beverage Emulsion. *Colloids Surf., A* **2008**, *315*, 47−56.
(44) Ahola, S.; Salmi, J.; Johansson, L. S.; Laine, J.; Österberg, M. Model Films from Native Cellulose Nanofibrils. Preparation, Swelling, and Surface Interactions. *Biomacromolecules* **2008**, *9*, 1273−1282.
(45) Kloser, E.; Gray, D. G. Surface Grafting of Cellulose Nanocrystals with Poly(Ethylene Oxide) in Aqueous Media. *Langmuir* **2010**, *26*, 13450−13456.
(46) Araki, J.; Wada, M.; Kuga, S.; Okano, T. Birefringent Glassy Phase of a Cellulose Microcrystal Suspension. *Langmuir* **2000**, *16*, 2413−2415.
(47) Majoinen, J.; Kontturi, E.; Ikkala, O.; Gray, D. Sem Imaging of Chiral Nematic Films Cast from Cellulose Nanocrystal Suspensions. *Cellulose* **2012**, *19*, 1599−1605.
(48) Bardet, R.; Cancé, C.; Horvatic, I.; Belgacem, N.; Bras, J. *Structural Colored Films Based on Nanocellulose*. Presented at TAPPI International Conference on Nanotechnology, Vancouver, Canada, 2014.
(49) Dong, X. M.; Kimura, T.; Revol, J.-F.; Gray, D. G. Effects of Ionic Strength on the Isotropic−Chiral Nematic Phase Transition of Suspensions of Cellulose Crystallites. *Langmuir* **1996**, *12*, 2076−2082.
(50) Osorio-Madrazo, A.; Eder, M.; Rueggeberg, M.; Pandey, J. K.; Harrington, M. J.; Nishiyama, Y.; Putaux, J.-L.; Rochas, C.; Burgert, I. Reorientation of Cellulose Nanowhiskers in Agarose Hydrogels under Tensile Loading. *Biomacromolecules* **2012**, *13*, 850−856.
(51) Cerolini, S.; D'Orazio, M.; Di Perna, C.; Stazi, A. Moisture Buffering Capacity of Highly Absorbing Materials. *Energy Build.* **2009**, *41*, 164−168.
(52) Zhang, Y. P.; Chodavarapu, V. P.; Kirk, A. G.; Andrews, M. P., Structured Color Humidity Indicator from Reversible Pitch Tuning in Self-Assembled Nanocrystalline Cellulose Films. *Sens. Actuators, B* **2012**.
(53) Chauve, G.; Bras, J., Industrial Point of View of Nanocellulose Materials and Their Possible Applications. In *Handbook of Green Materials*; World Scientific: 2014; pp 233−252.
(54) Ben Azouz, K.; Ramires, E. C.; Van den Fonteyne, W.; El Kissi, N.; Dufresne, A. Simple Method for the Melt Extrusion of a Cellulose Nanocrystal Reinforced Hydrophobic Polymer. *ACS Macro Lett.* **2011**, *1*, 236−240.

DOI: 10.1021/am506786t
ACS Appl. Mater. Interfaces 2015, 7, 4010−4018